Atomic-Scale Wear of Amorphous Hydrogenated Carbon during Intermittent Contact: A Combined Study Using Experiment, Simulation, and Theory

Vahid Vahdat,[†] Kathleen E. Ryan,[‡] Pamela L. Keating,[‡] Yijie Jiang,[†] Shashishekar P. Adiga,[§,∥] J. David Schall,[⊥] Kevin T. Turner,[†] Judith A. Harrison,[‡] and Robert W. Carpick[†,*]

[†]Department of Mechanical Engineering and Applied Mechanics, University of Pennsylvania, Philadelphia, Pennsylvania 19104, United States, [‡]Department of Chemistry, United States Naval Academy, Annapolis, Maryland 21402, United States, [§]Kodak Research Laboratories, Eastman Kodak Company, Rochester, New York 14620, United States, and [⊥]Mechanical Engineering Department, Oakland University, Rochester, Michigan 48309, United States. [∥]Present address (S.P.A.): Advanced Technology Laboratories, Lockheed Martin, Cherry Hill, New Jersey 08002.

ABSTRACT In this study, we explore the wear behavior of amplitude modulation atomic force microscopy (AM-AFM, an intermittent-contact AFM mode) tips coated with a common type of diamond-like carbon, amorphous hydrogenated carbon (a-C:H), when scanned against an ultra-nanocrystalline diamond (UNCD) sample both experimentally and through molecular dynamics (MD) simulations. Finite element analysis is utilized in a unique way to create a representative geometry of the tip to be simulated in MD. To conduct consistent and quantitative experiments, we apply a protocol that involves determining the tip–sample interaction geometry, calculating the tip–sample force and normal contact stress over the course of the wear test, and precisely quantifying the wear volume using high-resolution transmission electron microscopy imaging. The results reveal gradual wear of a-C:H with no sign of fracture or plastic deformation. The wear rate of a-C:H is consistent with a reaction-rate-based wear theory, which predicts an exponential dependence of the rate of atom removal on the average normal contact stress. From this, kinetic parameters governing the wear process are estimated. MD simulations of an a-C:H tip, whose radius is comparable to the tip radii used in experiments, making contact with a UNCD sample multiple times exhibit an atomic-level removal process. The atomistic wear events observed in the simulations are correlated with under-coordinated atomic species at the contacting surfaces.

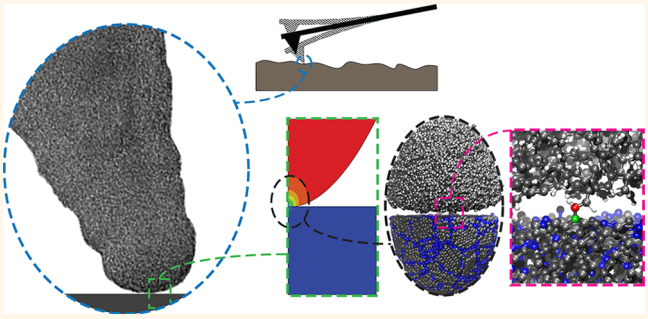

KEYWORDS: atomic-scale wear · AFM · tapping mode · contact mechanics · DLC · molecular dynamics · AIREBO

Wear is one of the main factors that hinders the reliable performance of probes for atomic force microscopy (AFM). This includes the widely used amplitude modulation (AM-AFM) mode, which involves hundreds of thousands of contact formation and breakage cycles per second and other intermittent contact AFM modes, such as PeakForce Tapping[1] AFM (also known as force mapping, a force–distance curve-based AFM) and dynamic plowing lithography (a scanning probe lithography technique).[2,3] To improve AFM probes' lifespan and reliability, materials with high wear resistance and low friction like amorphous hydrogenated carbon, a-C:H (a type of diamond-like carbon (DLC) film), have been used to coat Si AFM tips.[4,5] The frictional and wear behavior of DLC films with different compositions in sliding contact in various environments have been widely studied during the past two decades. The exceptional properties, such as high hardness, inertness, low friction coefficient, and wear rate of some DLC films in different environments, have made DLC a popular material for tribological applications like magnetic hard disks, mechanical seals, micro-electromechanical systems, and aerospace applications.[6] Conductive DLC is

* Address correspondence to carpick@seas.upenn.edu.

Received for review April 8, 2014 and accepted June 12, 2014.

Published online June 12, 2014
10.1021/nn501896e

proposed as an interfacial material to improve reliability in micro/nano-electromechanical switches,[7] as their performance is strongly affected by wear at electrode contact interfaces which must repeatedly open and close. Investigating single asperity wear in AM-AFM can help one understand wear in these applications.

The low friction coefficient and wear rates of DLC are mainly attributed to the formation of an amorphous sp^2-rich transfer layer between the interacting bodies. High contact temperatures and stresses can assist in this process.[11−13]

Some researchers have observed that a thermally activated mechanism (formulated by transition state theory or reaction rate theory) can describe the wear process of DLC. Jiang *et al.*[14] considered the effect of sliding speed on the wear of DLC by sliding a tungsten carbide ball on a DLC-coated disk in ambient air with 7% relative humidity (RH). They observed two different regimes: first, the wear rate decreased as the sliding speed increased from 0.048 to 0.25 m/s; second, in contrast to the first regime, the wear rate increased as the sliding speed increased from 0.25 to 0.45 m/s. To describe these opposing behaviors, they proposed a chemically activated debonding process at the tip of surface cracks in the film, promoting crack propagation and leading to wear *via* removal of the fragments produced. In the first regime, increasing the sliding speed resulted in less available time for reactive species, most probably oxygen and water, to migrate to the crack tip and consequently decreasing the rate of fragment removal. In the second regime, as the sliding speed increased, elevated contact temperature enhanced the migration and chemical reaction of the species with the atoms at the crack tip. It also increased the possibility of surface oxidization, resulting in an increase in the rate of crack propagation and fragment removal. Their experimental results were in agreement with a thermally activated model predicting the specific wear rate as an exponential function of the velocity-dependent temperature. The estimated apparent activation energy was approximately 27 kJ/mol, which corresponds to approximately 0.28 eV per atom.

In a single asperity sliding contact experiment, using a silicon-containing DLC-coated AFM tip scanning against SiO_2, Bhaskaran *et al.*[4] observed an atom-by-atom removal process and calculated an effective energy barrier of 1 ± 0.1 eV to remove one atom from fitting their experimental data to a thermally activated wear model proposed by Gotsmann and Lantz.[10] The corresponding effective activation volume was estimated to be 340 ± 200 Å^3. The effective activation volume was equal to $\xi \Delta V_{act}$, where ξ is the pressure dependence of the interfacial shear stress and was not reported by the authors.

Recently, Sha *et al.*[15] performed molecular dynamics (MD) simulations of a DLC hemispherical tip sliding across a flat DLC surface. They observed a gradual wear process which mainly follows Archard's wear law[16] and does not fit a thermally activated model. The sliding distance in their simulations was 39 nm, which may be particularly relevant for understanding the run-in period. Most of the nanoscale wear studies involve longer distances of sliding, resulting in different wear rates over the course of sliding for a single tip.[8,10] At the beginning, the wear rate is high; as the tip slides longer distances, the contact stress drops, resulting in a lower wear rate and possibly different wear behavior.

Despite the widely studied tribological characteristics of DLC in sliding contact, its wear behavior in surface interactions involving repeated contact formation and breakage without sliding, which is what occurs in AM-AFM, has not been widely investigated. In another study, Vahdat *et al.*[17] compared the wear behavior of a-C:H-coated and silicon-nitride-coated silicon probes in AM-AFM. Wear of a-C:H was characterized by gradual atom-by-atom removal, while plastic deformation and removal of clusters of atoms were the dominant wear mechanisms of silicon nitride.

In the present work, the wear behavior of a-C:H against ultra-nanocrystalline diamond (UNCD) samples using AM-AFM and molecular dynamics is further investigated. UNCD is selected as the sample because it is a hard and wear-resistant material that ensures that the wear is principally confined to the tip rather than the sample. Furthermore, it has a rough surface that can be used for blind tip reconstruction (BTR),[18] a mathematical procedure that is used to extract information about the geometry of the portions of the tip that interact with the sample during topographic image acquisition. The use of BTR is briefly discussed in the AM-AFM Wear Protocol section.

To complement the experimental work, MD simulations are used to investigate specific tip−sample interactions from the atomistic point of view. There are few studies simulating tip−sample interaction in AM-AFM.[19−22] In a novel approach to incorporate the cantilever dynamics into the MD simulations of the tip−sample interaction in AM-AFM, Kim *et al.*[19] simulated a half-sphere platinum tip ($R = 4$ nm) interacting with a platinum surface in a dynamic setup similar to AM-AFM. The dynamic effect, with some simplifications (constant acceleration and restoring force), was introduced by assigning an initial velocity and a constant restoring force to the tip at the proximity of the surface. To match the atomic mass of the simulated tip to the effective mass of an actual AFM cantilever and tip, they assigned an atomic mass of 100 ng to a region at the top of the tip. In this approach, they could predict the energy dissipation per cycle and extract local stiffness from force−distance curves. The proposed method provides a reasonable and comprehensive approach to study the effect of cantilever dynamics on the tip−sample interaction and *vice versa*. However, utilizing this approach in the current study adds complication

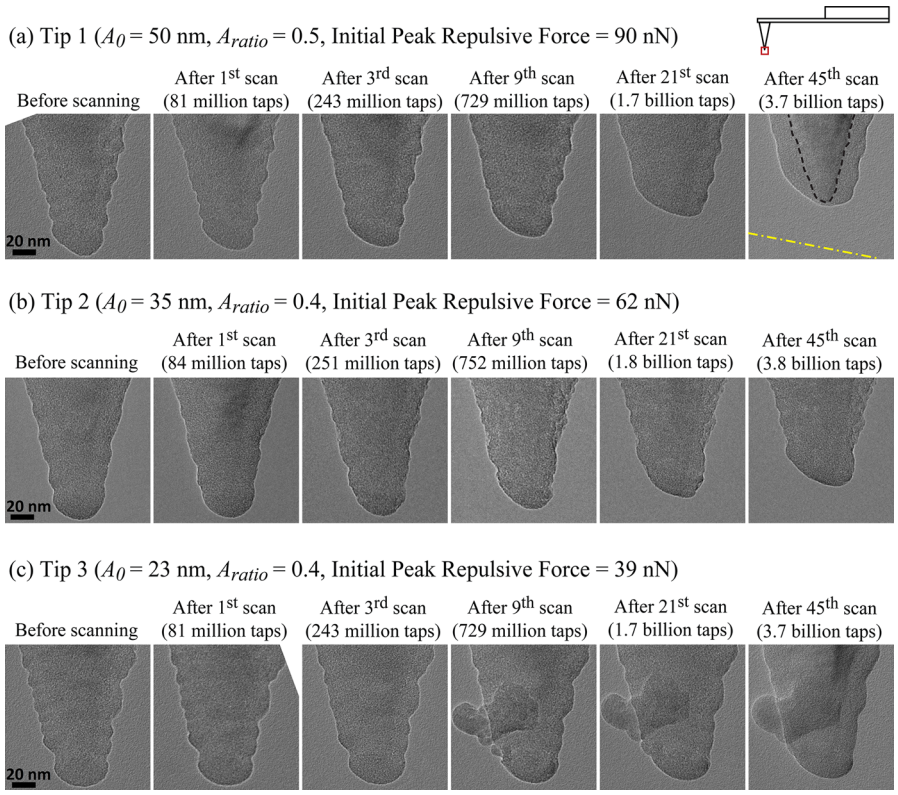

Figure 1. TEM images of the three a-C:H-coated silicon tips before any AFM imaging and just after completing 1, 3, 9, 21, and 45 AM-AFM images of the UNCD sample. (a–c) Correspond to three tips with different free oscillation amplitudes, A_0, and amplitude ratios, A_{ratio}. The black dashed line in the top right TEM image refers to the interface between the underlying silicon and a-C:H film, and the yellow dash-dotted line shows sample orientation (≈11°) with respect to the tip.

and computational expense, as the focus of the MD simulations here is the bond formation and breaking at the tip–sample interface under repetitive interaction. Therefore, the dynamics of the cantilever is ignored, and the tip–sample forces and displacement of the actual experiment are carefully calculated and then used in the simulations instead.

MD simulations are uniquely suited for the examination of atomistic processes, such as chemical bonding, because the positions, forces, and velocities on all atoms are known as a function of time. Modeling the AM-AFM process presents several challenges for MD simulations, namely, chemical reactivity and intermolecular forces, system size, simulation time, and repeated sequential contacts. To simulate chemical reactions as well as intermolecular forces between tip and surface, the widely used adaptive intermolecular reactive empirical bond order (AIREBO) potential for hydrogen and carbon was used.[23] Parallel MD simulations allow system sizes that are similar to the size of an AFM tip to be simulated.[24] For the AIREBO potential, as with others, computational time increases with the number of atoms. Thus, system size considerations must be carefully balanced by consideration of computational time. Finally, if multiple contacts are to be simulated, the total computational time of one contact cycle must not be prohibitive. Ideally, simulations should include the smallest number of atoms to keep the computational time low while at the same time be of sufficient size to capture the important deformation events caused by tip–sample contact. To keep the system size computationally accessible while still modeling the large radius of the simulated tip (15 nm), finite element (FE) modeling is utilized to identify portions of the tip and sample that can be excluded based on regions where the deformation during tip–sample contact is less than 15% of the maximum value. A detailed description of this approach is described in the Methods section.

RESULTS AND DISCUSSION

Wear scans, involving 45 AM-AFM imaging scans of a UNCD sample over a 1 × 1 μm^2 area, are performed with three different probes with a-C:H-coated silicon tips. The physical properties of these probes are listed in Table 1 of the Methods section. The AM-AFM experiments are performed using the Asylum MFP-3D AFM at a fixed relative humidity of 15% in a mixture of dry N_2 gas and humid air. The transmission electron microscopy (TEM) images of the three AFM tips before any scanning and after completing 1, 3, 9, 21, and 45 AM-AFM scans (1 × 1 μm^2, 512 × 512 pixels, 2 Hz scan rate) subjected to different peak repulsive forces are presented in Figure 1. The peak repulsive force refers to the maximum repulsive force that the AFM tip experiences on an oscillation cycle and is described in more details in the Methods section. The a-C:H

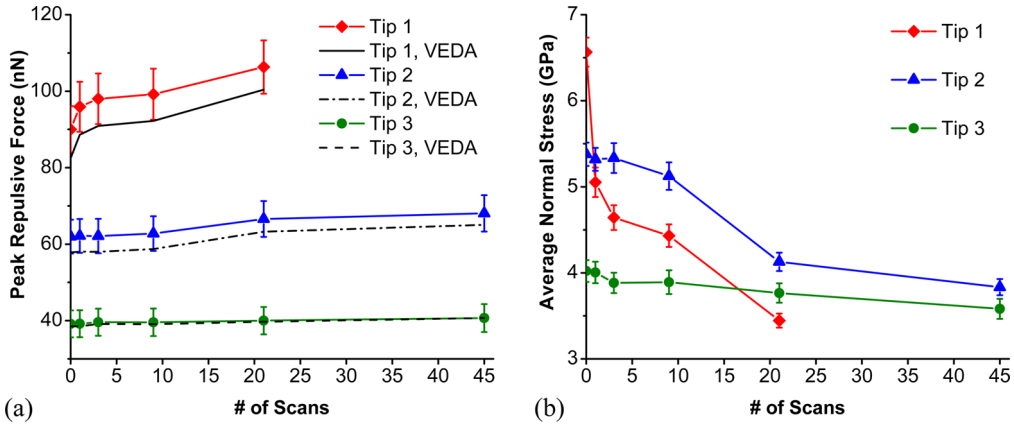

Figure 2. (a) Peak repulsive forces calculated for all three tips *vs* number of AM-AFM scans. The calculations rely on tip radii estimated by comparing 2D profiles captured from TEM and BTR of the height images to determine what specific portion of the tip apex is interacting with the sample during imaging and fitting parabola/circle (see Methods section). Peak repulsive forces are also calculated using VEDA for verification. (b) Average normal contact stress calculated for all three tips. The data point after 21 scans of the tip 1 is not shown as the a-C:H coating is completely removed after this point.

coating and its characteristics are also described in the Methods section. A custom-built probe holder was used for mounting the AFM probes in the TEM. However, it allowed only limited sample tilt. Therefore, it was not always possible to tilt the crystalline silicon to an orientation of high symmetry (*i.e.*, high diffraction contrast), resulting in no/low contrast difference between the Si and the a-C:H coating in the TEM images.

Each tip is subjected to a different number of interactions with the sample because the cantilever resonance frequency and consequently the drive frequencies are different from probe to probe. As well, the peak repulsive force experienced by the three tips (initially and throughout the experiment as the tips wear) are different, primarily due to using different free oscillation amplitudes, such that tip 1 consistently experiences the highest forces, and tip 3 the lowest. The forces are also affected by differences in tip radius, cantilever physical properties, and amplitude ratio used. There is a contamination particle attached to tip 3 that appears sometime between the 3rd and 9th scans. The contaminant is visible in the TEM images after 9th, 21st, and 45th scan and is not close to the region of the tip apex that interacts with the sample. Therefore, this particle does not introduce any error in the estimation of the tip radius and, consequently, the calculation of the force and stress. For the wear volume calculation, the original tip profile, which is clearly visible under the contaminant, is used.

The peak repulsive forces of the three tips as a function of the number of scans are plotted in Figure 2a. For each tip, there are two different plots corresponding to two different methods of calculating peak repulsive force. The first curve is obtained using a closed-form equation. For details, see the discussion of eq 4 in the Methods section. The second one is obtained using an online tool called Virtual Environment for Dynamic AFM (VEDA) developed by Melcher *et al.*[25] to verify the accuracy of eq 4. VEDA provides a more accurate estimation of forces as it does not involve mathematical approximations used to derive eq 4. In all cases, there is a close agreement between these two methods of force determination, and the VEDA results sit within the standard error of the forces calculated using eq 4. For all tips, a modest increase in the peak repulsive force is seen early in the wear test, followed either by a leveling off or a more gradual increase. The initial rapid increase is attributable to the rapidly increasing tip size at the outset of the wear test (refer to eq 4).

The calculated average normal stresses using Derjaguin–Müller–Toporov (DMT)[26] model corresponding to the peak repulsive forces are plotted in Figure 2b. The stresses calculated from the parabola/circle fits provide a lower bound for the contact stresses because the tip and sample roughness are ignored. The stresses evolve to a steady-state value that is nearly the same for all three tips ($\approx$3.6 $\pm$ 0.2 GPa) after a run-in period, even though the peak repulsive forces are quite different (98, 64, and 40 nN on average).

Wear Volume and a Preliminary Study of Humidity Effects. Figure 3a shows the wear volume as a function of the number of taps. The wear volume is calculated by integrating over the tip's 2D profile using the method of disks.[8] This integration approach assumes that the tips are circularly symmetric at each resolved height. It is apparent that the tips with higher peak force and initial normal stress (as shown in Figure 2) experience more wear. This indicates that the wear process is initially stress-controlled. Eventually, the wear rate of tips 2 and 3 reduce as the stress reduces; on the basis of these and other tests, we expect the wear rate for tip 1 would also reduce with continued testing. However, even though the contact stresses of all three tips converge to the same value as discussed above, the wear rate continues to be correlated with the initial stress, with the wear rate higher for higher initial stresses.

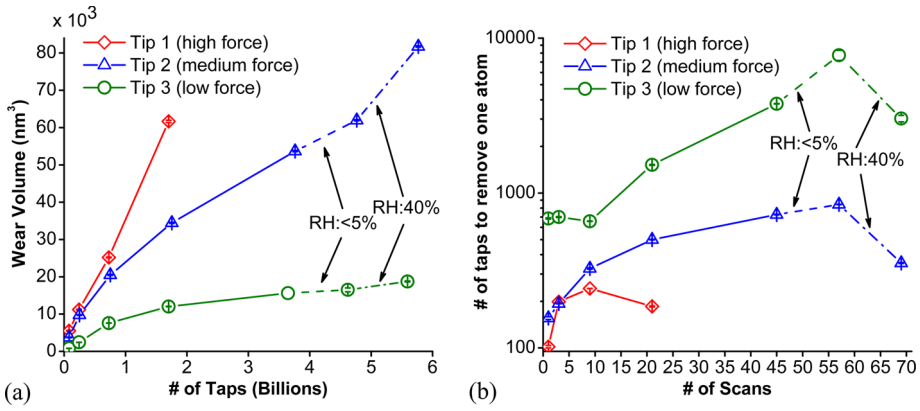

Figure 3. (a) Wear volume as a function of number of taps in a mixture of air and nitrogen gas with 15% RH (except as indicated). The standard error of the measured wear volume is negligible in comparison to the wear volume itself and is thus difficult to see on the plots. The wear volumes of tips 2 and 3 in <5% RH (dashed line) and in 40% RH (dash-dotted line) are also plotted. (b) Average number of taps to remove one atom as the tip wears. The data point after 21 scans of tip 1 is not shown as the a-C:H coating is completely removed after this point.

This suggests that the wear mechanism is somehow accelerated due to having higher initial stresses. The MD simulations discussed in the following section show that wear can be initiated and then continued through bonding across the interface of atoms at the surfaces of the tip and sample which are under-coordinated. Therefore, it is possible that the higher the initial stress, the more under-coordinated atoms are exposed or created, and this leads to higher successive wear rates. This implies that there is a history dependence to wear, such that a high wear history leads to surface atoms that are less stable and thus more prone to successive wear events. Such a mechanism can explain why tips that eventually have similar contact stresses retain very different rates of wear.

TEM images show no sign of fracture or plastic deformation, supporting the hypothesis that a gradual wear process is occurring. The gradual wear process can also be deduced from Figure 3a, which shows a gradual change in the wear volume. This gradual wear process could be reasonably described as an atom-by-atom removal process: it can be seen in Figure 3b that the average number of taps (between successive TEM images) needed to remove one atom varies from 100 to 8000. Even at the highest rate, this is a very slow process. However, as in AM-AFM, tip−sample contact formation and breakage cycles are on the order of a few hundred thousand times per second (here, ~300 000 per second), the wear volume becomes significant after several billion taps over the course of the wear experiment (or of typical imaging sessions where several images are to be acquired). This behavior suggests utilizing a scheme that can describe this gradual atom removal, for example, reaction rate theory, which is discussed later. The worn volume, density, and the hydrogen content of the a-C:H film is used to calculate the number of atoms removed between the two successive TEM images required to plot Figure 3b.

Overall, the experimental results show that the nanoscale wear in a-C:H-coated AM-AFM probes can be significant. However, tip wear can be significantly reduced by choosing appropriate experimental parameters. This is discussed in detail by Vahdat and Carpick in a study to limit contact stress in AM-AFM.[27] Both panels a and b of Figure 3 demonstrate the dramatic difference between the wear of tips 1 and 3. In Figure 3b, we can clearly see that the average number of tip−sample interactions required to remove one atom from tip 3 is an order of magnitude more than tip 1.

A preliminary study of the effect of humidity was also conducted after scan 45 (the humidity was the same for all three tips up to scan 45). For tip 2 and tip 3, the relative humidity was varied. From scan 1 to scan 45, the humidity was 15%; from scan 46 to 57, it was less than 5%; and from scan 58 to 69, it was 40%. The wear rate is seen to change at different relative humidities; specifically, the presence of moisture promotes the wear mechanism/s and consequently accelerates wear. The effect of humidity can be seen more clearly in Figure 3b. As the humidity increases, fewer tip−sample interactions are required to remove one atom from the tip on average.

This could be due to the tribochemical effect that water has on bond formation between atoms at the surface of the tip and the sample. Based on previous studies, the macroscopic friction coefficient and consequently the wear rate of a-C:H increases as RH increases in the environment.[28−33] Increasing the RH results in the physisorption of water on the tip and sample surface. During the making and breaking of the contact, the high contact stresses might promote the dissociative chemisorption of water or oxygen molecules at unsaturated sites formed by breaking C−C and C−H bonds at the surface. A similar mechanism has been observed for diamond and tetrahedral amorphous carbon films in macroscopic sliding contact in humid environments.[34,35] In the present experiments, the RH is controlled by administration of dry nitrogen to the AFM chamber which is initially filled with

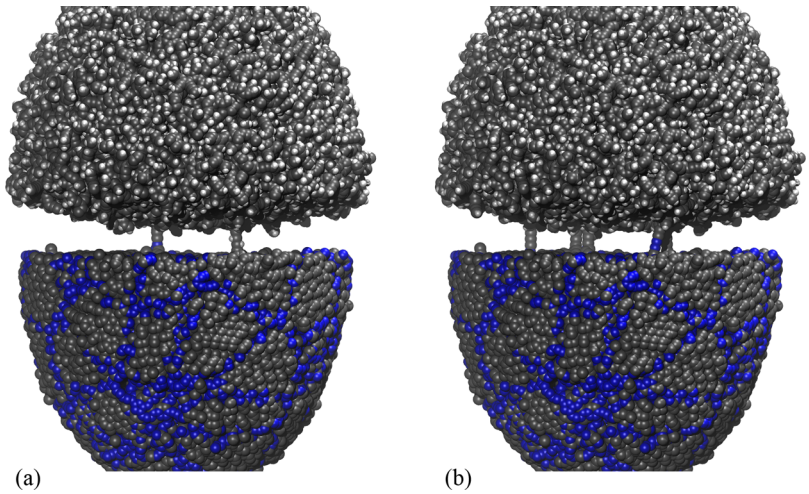

Figure 4. Snapshots of the hydrogenated a-C:H tip retracting from UNCD surface after the first contact with (a) 20 nN and (b) 55 nN peak contact force. In the a-C:H tip, gray and small white spheres represent carbon and hydrogen atoms, respectively. In the UNCD substrate, gray and blue spheres represent carbon atoms in diamond grains and grain boundaries, respectively.

laboratory humid air. The lower the RH is, the higher the percentage of nitrogen in the air−nitrogen gas mixture is. As oxygen and water are removed from the test environment, these tribochemical interactions are reduced.

Molecular Dynamics Observations. The gradual removal of atoms during the wear process and the direct relationship between the contact stress and wear rate observed in the experimental results are further supported by MD simulations. MD simulations have the advantage of providing a full atomically resolved picture of the contact behavior while resolving all positions, velocities, forces, and bonding states of the atoms. A key challenge of this approach is that the simulations can only be conducted for a small number of interaction cycles, while the experiments involve billions of cycles. Thus, the simulations are not to be regarded as a full representation of the evolution of the experimental tip. Rather, the simulations provide examples of possible interfacial behavior that can occur. Given the extent to which the AIREBO potential has been tested and validated in many different reactive situations, we can regard the observed events as reasonable ones to consider in explaining the experimental results.

A simulation of three consecutive contact and retraction cycles between an a-C:H tip (with 15 nm radius comparable to the initial size of the tips used for the experiments) and a UNCD surface are carried out. Using separate simulations, two different peak contact forces, 20 and 55 nN, are attained prior to retraction of the tip. These forces are chosen to reproduce the contact stress of tip 3 and tip 1, respectively. For the case of 20 nN contact force and the 15 nm tip radius, the average contact stress of the MD tip and sample is approximately 4.6 GPa calculated using continuum mechanics. This is close to the initial average contact stress of the experimental tip 3 ($\approx$4.0 $\pm$ 0.1 GPa) which has the lowest wear volume of the three tips tested. The average contact stress for the case of 55 nN is approximately 6.4 GPa, close to the initial average contact stress of the experimental tip 1 ($\approx$6.6 $\pm$ 0.2 GPa) which has the highest wear volume of the three tips tested. Details of the MD simulations are presented in the Methods section. Note that the tip structure used has unsaturated atoms at its surface. As we are most interested in wear events that happen during the extended period of cycling, this structure is desirable, as it provides a reasonable representation of an unpassivated tip or one that has already been undergoing interfacial bond-breaking interactions.

Figure 4 shows the tip during retraction from the sample after the first contact cycle for both the 20 and 55 nN peak contact forces. The first key point to note is that the overall integrity of the tip is preserved. In these contact cycles, and throughout the simulation, there are no occurrences of large-scale fracture or plasticity. Rather, the only wear events that occur involve small numbers of individual atomic bonds forming and then breaking across the interface. This is in agreement with our interpretation of the gradual wear of the AFM tips discussed above and published previously.[17,27] Atom-by-atom transfer is observed through the formation of individual bonds, some of which result in the transfer of single atoms between the tip and sample. Following the bond formation, chains of sp-coordinated carbon atoms are formed as the tip pulls away from the sample. These linkages break when sufficient force is applied by the retracting tip. These long carbon chains would not be expected to survive in an air environment and may not be expected to occur even in vacuum; rather, we hypothesize that this specific aspect of the simulation occurs as a result of the short-range nature of the covalent portion of the AIREBO potential. The short cutoff distance of Brenner's REBO potential

TABLE 1. Cantilever Properties and Experimental Parameters Used for Wear Experiments

cantilever:PPP_NCHR (nanosensors), 20 nm a-C:H coating	initial tip radius (nm)	spring constant (N/m)	resonance frequency (kHz)	free oscillation amplitude, A_0 (nm)	amplitude ratio, A_{ratio}
tip 1	19	43 ± 2	308.6 ± 0.1	50.0 ± 1.3	0.50 ± 0.03
tip 2	21	48 ± 2	318.3 ± 0.1	35.0 ± 1.0	0.40 ± 0.04
tip 3	27	42 ± 2	308.6 ± 0.1	23.0 ± 1.2	0.40 ± 0.07

TABLE 2. Number of Hydrogen and Carbon Atoms Transferred between the a-C:H tip and UNCD Sample during Each of the Three Consecutive Contact Cycles with 20 nN and 55 nN Contact Force[a]

	20 nN Contact Force				
	atoms removed from a-C:H tip		atoms removed from UNCD surface		
contact cycle	hydrogen	carbon	hydrogen	carbon	cumulative atom loss from original tip/surface
1	2	2	0	2	4/2
2	0	1*	1**	2**	1/1
3	0	0	0	0	1/1
	55 nN Contact Force				
	atoms removed from a-C:H tip		atoms removed from UNCD surface		
contact cycle	hydrogen	carbon	hydrogen	carbon	cumulative atom loss from original tip/surface
1	2	5	0	0	7/0
2	2	3	0	1**	11/0
3	1	5	1**	1	15/0

[a] Asterisks for the second and third contact cycles show where the atoms originated, indicating that some material is simply transferred between the tip and surface without accumulating significant wear. *Originated from the surface. **Originated from the tip.

(and thus the AIREBO potential) causes the force to break covalent bonds to be larger than that predicted by density functional theory (DFT) calculations. This has been reported by Pastewka *et al.*[36] and was verified by comparing REBO calculations to DFT. While conclusions about the quantitative value of the forces required to break the atomic linkages cannot be gleaned from the simulations presented here, the simulations do reveal the qualitative bond-forming processes that occur when a-C:H and UNCD are brought into contact.

Table 2 lists the number of hydrogen and carbon atoms that are removed from the tip and sample following the three contact cycles for both 20 and 55 nN peak contact forces. The cumulative atom loss from original tip/surface is also listed. The hydrogen atoms removed from UNCD sample originally belong to the tip and were transferred to the sample during the previous contact cycles. In the case of 20 nN contact force, although the tip loses four atoms during the first contact cycle, it regains three of them during the second one. In other words, we observe atoms moving back and forth between the tip and sample without significant accumulated wear from one surface to the other. In contrast, for the 55 nN contact force, the tip has a cumulative loss of 15 atoms; only three atoms are transferred back and forth during the multiple contacts. The larger number of atom loss in this case indirectly confirms that the contact stress (in its continuum definition) plays a pivotal role in the initiation of the wear process.

Two specific instances of atom transfer identified *via* the simulations are depicted in Figure 5. In both cases, under-coordinated, sp-hybridized carbon atoms (coordination number of 2) from the a-C:H tip form bonds with a sp-hybridized carbon atom in the UNCD and ended up with a coordination number of 3 in the UNCD sample. In one case, the carbon bond is on the surface of a diamond grain. In the second case, the carbon atom is within a grain boundary. Interestingly, in the second case, atoms of the tip are pushed aside as a result of the contact interactions, and a carbon atom that was not originally at the surface of the a-C:H ends up forming a bond with a carbon atom in the UNCD sample. In general, in all instances of atom transfer from the tip to the sample, the coordination number is increased by one.

As mentioned above, these two instances of bond formation represent possible mechanisms that may be present in the AM-AFM. A substantially larger number of simulations would be required to more completely catalog the range of atomic wear processes that may be occurring in the experiment. Regardless, the principal observation of gradual, atomic-scale wear, as opposed to plastic deformation, nanoscale fracture, or a complete lack of wear, is consistent with the experimental observations and thus provides support

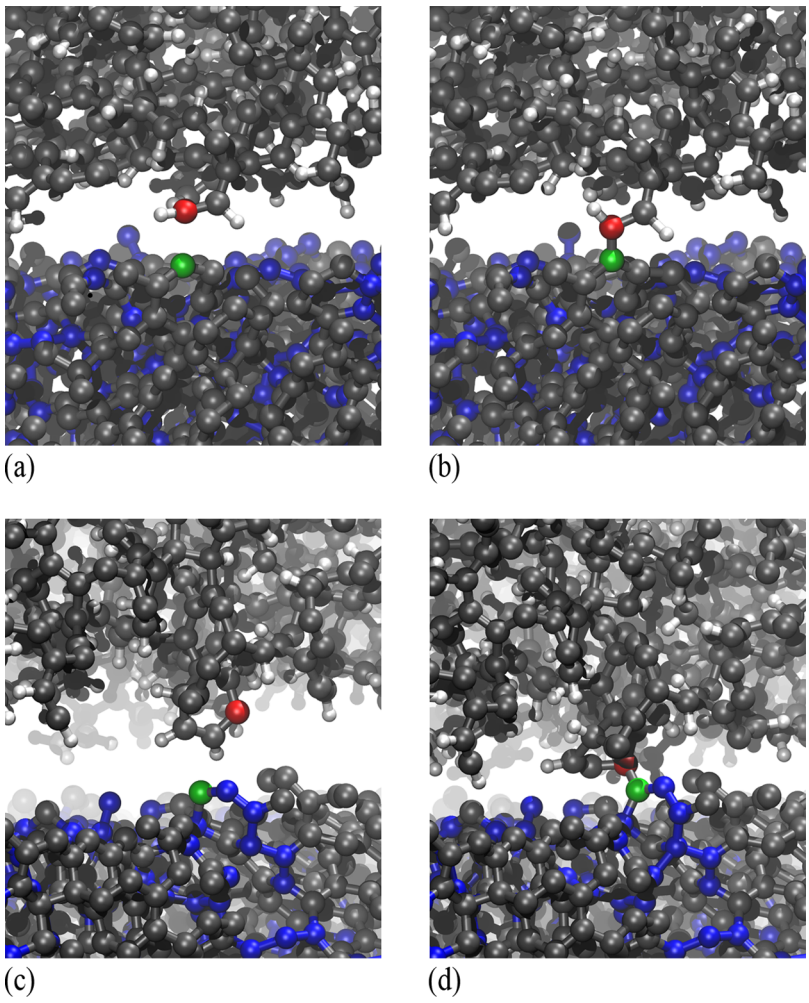

Figure 5. Two specific instances of the bond formation between the tip and surface atoms. (a,b) Depict instances before and after bond formation, respectively, between a carbon atom on the tip and a carbon atom on a diamond grain on the surface. (c,d) Depict instances before and after bond formation, respectively, between a carbon atom on the tip and a carbon atom on the surface grain boundary.

for the notion that the accumulated tip wear is a result of atomic-level wear processes.

Reaction Rate Theory Applied to AM-AFM. The gradual, atom-by-atom wear processes proposed to explain the experimental results, which are further supported by the MD simulations, suggest that the wear of a-C:H in AM-AFM could be described by a thermally activated mechanism.[4,10,37] In this mechanism, the transfer of atoms from the tip to the sample are pictured as transferring from a local (metastable) equilibrium state at the bottom of a potential well to another local equilibrium state with a local minimum potential energy by overcoming an energy barrier (Figure 6). In this picture, the pathway along the reaction coordinate will be the one with the lowest energy required for the transition among all other possible pathways. The intermediate state at the top of the energy barrier is called the activated state. The activated state is assumed to be unstable just along the reaction coordinate and is stable in all other directions. In other words, the atom of interest has one degree of freedom,

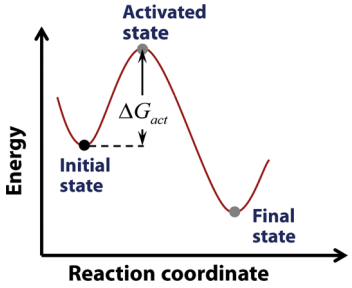

Figure 6. Atom transfer from tip to the sample is simulated by a double-well potential. ΔG_{act} is the energy barrier that should be overcome by the tip atom to transfer from initial to final equilibrium state.

and if it makes it to the activated state, there is a probability that it goes forward and completes the transition; the forward reaction is assumed to dominate due to the lower energy of the final state.

The application of reaction rate theory to nanoscale wear is discussed extensively by Jacobs *et al.*[37] Briefly, the rate of atom loss or the number of atoms that can

successfully pass the energy barrier per second, $\Gamma_{\text{atom loss}}$ (s^{-1}), depends exponentially on a stress component promoting the reaction as follows:[38]

$$\Gamma_{\text{atom loss}} = \left\{\Gamma_0 \exp\left(-\frac{\Delta U_{\text{act}}}{k_B T}\right)\right\} \exp\left(\frac{\sigma \Delta V_{\text{act}}}{k_B T}\right) \quad (1)$$

where Γ_0 is the attempt frequency which is in the order of atomic vibration, $\approx 10^{13}$ Hz; ΔU_{act} is the internal energy of activation which is the energy difference between the activated and initial states and is reduced by imposing stress, σ is a stress component or average stress value reducing the energy barrier and thus promoting wear; ΔV_{act} is the activation volume; k_B is Boltzmann's constant; and T is the absolute temperature.

The accurate application of eq 1 to the nanoscale wear strongly depends on the choice of stress component, which should have the highest impact on the wear process. In AM-AFM, all the stress components are at their maximum value at the closest tip−sample distance in a tapping cycle, which is a result of the repulsive force reaching its maximum value. Understanding the possible mechanism that results in atom removal from the tip can help to better choose the stress component in charge of pushing the process forward. An atomistic picture can be helpful in this context. The cyclic loading and unloading of the tip atoms can result in stress-assisted formation of bonds across the interface,[38,39] for example, between pairs of carbon atoms. This process may be more likely to occur if one or both of the C atoms are unsaturated or have a dangling bond present. However, these newly formed bond(s) between the tip and sample atoms are not necessarily stronger than the bonds that keep the atom(s) connected to the tip, unless the tip atom(s) are able to adopt a low enough coordination state (*i.e.*, a strong enough bond across the interface) that cannot further support their connection to the tip. Therefore, the rate-limiting factors should be both the bond formation across the interface and the lowering of the coordination state of the tip atoms.

Because of a-C:H's amorphous structure, there is no preferred direction for bonding; therefore, any stress component can potentially lower the coordination state of the tip atoms. However, the stress component with the largest value will be the most likely one to contribute. In the Hertzian stress distribution, the normal compressive stress at the interface is the largest (Figure 4.3 of "Contact Mechanics" by Johnson[40]), and for this reason, we choose it as the wear-promoting stress component in eq 1. It should be noted that interfacial shear stress is minimal in AM-AFM as there is no imposed sliding, and so shear stresses at the interface are not considered here as being likely to promote wear.

To successfully apply eq 1 to AM-AFM, a few simplifying assumptions are required. First, a single value for the normal contact stress is used. In fact, the normal contact stress is not uniform across the interface. In a Hertzian contact, the normal stress is maximum at the center of the contact and in a parabolic fashion approaches zero at its periphery. This is in addition to the fact that the tip and sample roughness and atomic detail are ignored in the Hertz model. However, for simplicity, we assign a single value for the stress experienced by the tip atoms at the interface between two successive TEM images by assuming that all atoms are subjected to the average normal stress across the interface. Not utilizing this assumption would require expressing the rate of atom loss as a function of the radial position at the contact and a subsequent integration. However, recent modeling has suggested that the normal stress distribution for a nanocontact between amorphous materials does not strictly follow the Hertzian distribution at the atomic scale (Figures 3 and 4 of the paper by Luan and Robbins[41]). Rather, the normal stress is more evenly distributed over the contact area in comparison to the Hertzian continuum model or a tip with crystalline structure. Significant fluctuations in the normal stress occur due to variations in atomic positions. In principle, this could be accounted for by using the details of the MD simulations, but we would not be able to connect the results directly to the experiments since the specific atomic structure of the tip and sample in the experiment is not known.

Second, we assume that the average normal stress stays constant over the contact time for each cycle. In AM-AFM, the tip−sample interaction force and consequently the stress change during the contact time at each tapping cycle (this is not an issue in contact mode AFM which is performed at a constant force).

The error arising from these two assumptions is difficult to determine due to a lack of knowledge of the contact stresses at the atomic scale in the experiment. However, by using the peak stress during the time of interaction, as opposed to the mean stress during the interaction, the calculations likely represent an upper bound to the stresses that are experienced. This assumption thus helps alleviate error arising from ignoring tip and sample roughness and atomic structure.

The rate of atom loss of eq 1 can then be calculated using the following relationship, which normalizes the number of atoms being removed in an interval by the contact area and contact time:[38]

$$\Gamma_{\text{atom loss}} = \frac{V_{\text{wear}} \times \rho_{\text{bulk}}}{A_{\text{cont}} \times \rho_{\text{surf}} \times t_{\text{cont}}} \quad (2)$$

where V_{wear} is the incremental wear volume measured by subtracting tip volume calculated from the consecutive TEM images; ρ_{bulk} and ρ_{surf} are the number density of the bulk and surface of the material which for a perfectly amorphous material; ρ_{surf} can be approximated by $\rho_{\text{bulk}}^{2/3}$; A_{cont} is the contact area which could

be calculated using the peak repulsive force and DMT contact model; and t_{cont} is the contact time between the tip and sample which in AM-AFM can be estimated by multiplying the contact time in an oscillation cycle by the number of taps in the given interval of the calculated wear volume. Therefore, eq 2 can be rewritten for the case of AM-AFM as follows:

$$\Gamma_{\text{atom loss}} = {\rho_{\text{bulk}}}^{1/3} \times \frac{V_{\text{wear}}}{A_{\text{cont}} \times \#\text{ of taps} \times t_{\text{per cycle}}} \quad (3)$$

As mentioned above, each incremental wear volume in the experiments is calculated by subtracting the estimated tip volumes of two successive TEM images. On the other hand, we evaluate average contact stress, contact area, and contact time using the tip radius estimated at every TEM image; therefore, for a given incremental wear volume, we have two values for these three parameters. Thus, the average of the values taken from successive images is used in eqs 1 and 3. The value of ρ_{bulk} is calculated to be approximately 144 $\pm$ 5 atoms per nm^3, using the measured hydrogen content and the density of the a-C:H here (see the Methods section for details). Approximately 85 of these atoms are carbon and 59 of them are hydrogen.

As with the average normal stress, the contact area is also assumed to be constant over the contact time in a single contact cycle. Unfortunately, there is no reliable closed-form equation to calculate the contact time in a single tapping cycle. However, one can numerically solve the equation of motion of the cantilever's first flexural mode using a point-mass spring model with one degree of freedom.[42] One can also use VEDA to calculate the contact time by providing AM-AFM scanning parameters, tip and sample material properties, and an appropriate contact mechanics model. We have verified that the estimated contact time using VEDA is in close agreement with our custom MATLAB script that simulates a cantilever approaching and retracting from a surface in AM-AFM mode using the point-mass model. The calculations presented in this work use the contact time estimated using VEDA.

Figure 7 plots the rate of atom loss *versus* average normal stress for the three a-C:H-coated tips. Also plotted is an exponential fit (solid line) which agrees within error with the data, indicating that an exponential relationship between the reaction rate and average normal stress is possible. Note that a linear function produces a much worse fit and is completely unreasonable when forced to intersect the origin. The calculated activation volume associated with the best exponential fit is 5.5 $\pm$ 0.8 Å^3, and the activation energy is 0.8 $\pm$ 0.8 eV. The activation volume is on the order of an atomic volume, and the activation energy is on the order of the energy required for nonbonded species to form a bond. The large uncertainty in the activation energy results mainly because only a limited range of

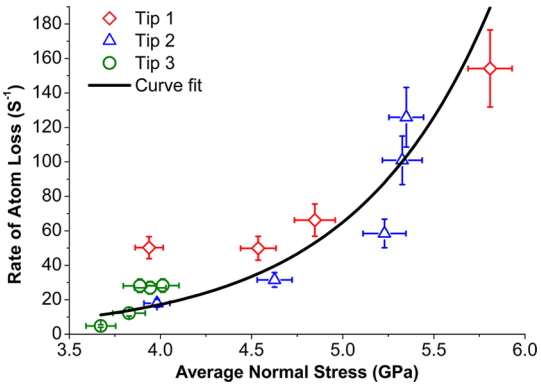

Figure 7. Calculated rate of atom loss plotted as a function of average normal stress. An exponential function is fit to the data points.

stress values could be accessed in these experiments and the experiments could only be performed at a single temperature. An accurate determination of the activation energy could be more readily determined by conducting experiments at different temperatures.[37]

Regardless, the estimated range of activation energies is consistent with the values predicted by Jiang *et al.*[14] (0.28 eV per atom) and Bhaskaran *et al.*[4] (1.0 $\pm$ 0.1 eV) for sliding-induced wear of DLC. Jiang *et al.* did not report an activation volume, but Bhaskaran *et al.* calculated the effective activation volume for the silicon-containing DLC to be 340 $\pm$ 200 Å^3 which, as discussed above, cannot be converted to a true activation volume as they did not measure the pressure dependence of the interfacial shear stress. While the physical interpretation of the activation volume is subject to debate, it is often associated with the volume on which the stress does work to displace atoms to lead to the activated state. In this picture, the atomic-scale volume determined from these experiments is consistent with an atomic-scale wear process, in agreement with the processes seen in the MD simulations.

CONCLUSIONS

The wear behavior of three a-C:H-coated silicon probes is examined under different experimental parameters in AM-AFM (intermittent contact) mode. It is observed that wear of a-C:H in AM-AFM is a gradual process; however, depending on the experimental parameters, the accumulated wear can eventually be significant due to the large number of tip−sample interactions per second (~300 000). MD simulations, using a simulation volume optimized through finite element simulations, observe atomic material transfer events, which occur more at increased maximum contact force, consistent with experiments. The wear events exclusively occur between under-coordinated atomic sites. The rate of wear can be modeled as a stress-assisted thermally activated process, which predicts an exponential dependence of the rate of atom

loss on the mean normal stress at the peak force. The experimental wear rate plotted as a function of average normal contact stress is found to be consistent with the predictions of this model. Finally, the presence of water in the environment is seen to significantly increase the wear rate in the experiments. However, further investigations are required to fully understand the effect of environmental species on the wear processes.

METHODS

The DLC coating, nominally 20 nm thick (as measured by TEM), was deposited on silicon probes (PPP_NCHR, Nanosensors) using the plasma immersion ion implantation and deposition process by Dr. K. Sridharan (University of Wisconsin—Madison, Center for Plasma-Aided Manufacturing).[43] The hydrogen content of DLC film is about 41 ± 2 at. % and a density of 1.79 ± 0.1 g/cm^3, based on secondary ion mass spectroscopy experiments and X-ray reflectivity measurements (Evans Analytical Group, Sunnyvale, CA) performed on DLC films deposited on flat substrates using the same deposition system and conditions as the films deposited on the tips. Approximately 50−70% of the carbon structure is in sp^3 state. Thus, this particular DLC is considered to be an amorphous hydrogenated carbon film (a-C:H).[6] Hardness is typically 13 GPa, and the measured Young's modulus varies from 120 to 180 GPa.[43] Poisson's ratio is assumed to be about 0.3.[44]

The counter surface was a UNCD[8,9,45] film deposited on a Si substrate (Aqua 25 with about 7 nm rms roughness, from Advanced Diamond Technologies, Inc.).

AM-AFM Wear Protocol. To perform consistent wear experiments, an AM-AFM wear protocol, described in detail by Vahdat *et al.*,[17] is followed. In summary, the experiments involve initial assessment of the AM-AFM probes' cantilever and tip. Resonance frequency and quality factor of the cantilevers are measured by an AFM instrument (Asylum MFP-3D); the length and width of the cantilever is measured by a white-light profilometer (Zygo NewView 3100), and the cantilever spring constant is estimated using Sader method.[46] Before performing any wear scan, using high-resolution TEM, AFM tips are imaged to assess their morphology and discard the ones with unusual tip shapes or contamination. After initial assessments, the free oscillation amplitude A_0 and amplitude ratio A_{ratio} (tapping amplitude A divided by A_0) for each tip are chosen depending on the desired initial peak repulsive force using the following equation:

$$F_{peak}^{rep} \approx 2^{1/8}3^{-1/4}\pi^{3/4}(E^*\sqrt{R})^{1/4}(k/Q)^{3/4}A_0^{9/8}A_{ratio}^{9/8} \times \left\{(-1+\Omega^2)Q+\sqrt{\frac{1}{A_{ratio}^2}[\Omega^2+(1-\Omega^2)^2Q^2]-\Omega^2}\right\}^{3/4} - F_{adhesion}/2$$

$$\text{where } \frac{1}{E^*} = \frac{(1-\nu_t^2)}{E_t}+\frac{(1-\nu_s^2)}{E_s} \text{ and } F_{adhesion} = -2\pi wR \quad (4)$$

where E^* is reduced Young's modulus; R is the tip radius; k is the cantilever spring constant; Q is the quality factor; Ω is drive frequency ω divided by resonance frequency ω_0; $F_{adhesion}$ is the adhesion force; E_t and E_s are Young's moduli for the tip and sample; ν_t and ν_s are Poisson's ratios for the tip and sample; and w is the work of adhesion.[47] In an oscillation cycle, as the tip approaches the sample, it goes through different force regimes which start with long-range van der Waals and possibly intermediate-range capillary attractive forces. As the tip begins to indent the sample, short-range repulsive forces begin to slow down the tip until it comes to rest. At this point, the tip feels the maximum normal repulsive force. The peak repulsive force is the most relevant force to the study of wear in AM-AFM. If there is any damage to the tip in an oscillation cycle, it is most likely to happen at this point where the tip is farthest from the cantilever rest position.

The work of adhesion between the a-C:H and UNCD, required to estimate adhesive force used in the peak repulsive force equation, is estimated by performing pull-off force measurements using the a-C:H-coated contact mode probes. Using three different probes, a total of 450 force−distance curves are acquired at a fixed relative humidity of 15%. Five different random locations of the UNCD surface are sampled 30 times summing up to 150 force−distance curves for each probe. The calculated work of adhesion is 31 ± 10 mJ/m^2, which is an average of the 450 measured work of adhesion using the DMT contact mechanics model. A justification for using DMT model, for the case of a-C:H and UNCD, is discussed by Vahdat *et al.*[17]

The cantilevers are driven at their resonance frequencies, and their free oscillation amplitude and amplitude ratio are kept constant to avoid considerable change in peak repulsive force during the experiment. However, as the tip radius increases through wear, the peak repulsive force because of its dependence on the tip radius (eq 4) slightly increases (Figure 2). After determination of the three sets of free amplitudes and amplitude ratios for three different probes with a-C:H-coated silicon tips, wear scans, involving 45 AM-AFM imaging scans of the UNCD sample over a 1 × 1 μm^2 area, are performed. The AM-AFM experiments are performed using the Asylum MFP-3D AFM at a fixed relative humidity of 15% in a mixture of dry N_2 gas and humid air. The AM-AFM parameters, which are listed in Table 1 along with the cantilever properties, are chosen so that the scanning occurs in the repulsive regime. The material properties used for calculating the peak repulsive force and the average normal stress are summarized in Table 3.

Two consecutive extra sets of 12 scans in less than 5% RH and in 40% RH are performed on two of the tips with some a-C:H coating left after the 45 wear scans to investigate the effect of moisture on the wear rate. Periodic TEM images are acquired after completing 1, 3, 9, 21, and 45 AM-AFM scans of all three tips and also after 57 and 69 scans of the two tips studied in different relative humidity. The TEM images are used to estimate the tip radius by fitting circles and parabolas to the tip profile and averaging the resulting radii. The tip profile is obtained by tracing the edges of the tip boundaries using a custom MATLAB script. This 2D tip profile is along the cantilever long axis as TEM electron beam gets blocked by the probe carrier chip in other directions. To determine the regions of the tip apex that interact with the sample, we have matched the profile obtained from applying BTR to the AM-AFM topography image acquired right before TEM imaging. The above-mentioned circle or parabola then is fitted to the regions of the tip that the TEM and BTR profiles overlap. BTR is performed using commercial software (SPIP, Image Metrology A/S). More details of these procedures can be found in the work by Vahdat *et al.*[17]

Finite Element Analysis To Determine the Optimum Tip and Sample Shape for MD Simulations. An axisymmetric finite element model of an a-C:H AFM tip and a UNCD substrate is built using ABAQUS program. The tip radius and height are chosen to be 15 and 30 nm, respectively (Figure 8a). The elastic properties of the tip and sample materials are taken from Table 3. Elements of type CAX4R, a 4-node bilinear axisymmetric quadrilateral element with reduced integration and hourglass control, are used. The FE model has 84 984 elements in total. The mesh convergence has been achieved by systematically increasing the mesh density until the normal stress distribution at the contact as a

TABLE 3. Material Properties Used in Calculations of the Contact Properties

	Young's modulus (GPa)	Poisson's ratio
UNCD	790 ± 30[48]	0.057 ± 0.038[48]
a-C:H	150 ± 30[43]	0.3 ± 0.05[44]

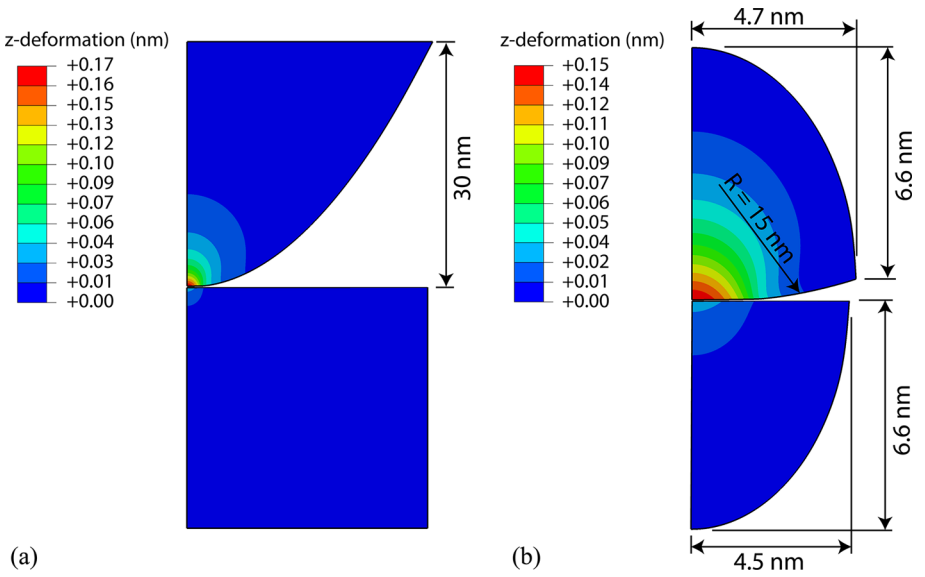

Figure 8. Deformation field of the (a) original and (b) modified axisymmetric FE model of the a-C:H tip and UNCD sample. The dimensions correspond to the geometries before contact.

function of the mesh density reached a plateau. The bottom of the UNCD surface is constrained in both the radial and vertical directions. The tip and substrate contact is nonadhesive and frictionless. A vertical displacement of 0.21 nm is applied on the top boundary of the tip to approximately create 70 nN (an upper bound to the 20 and 55 nN used in MD simulations) contact force. The two contact forces in the MD simulations are chosen based on two criteria. The 55 nN contact force is chosen to be comparable to the values of the initial peak repulsive forces in the experiments (35−96 nN). The 20 nN force is chosen in a way that it results in a similar indentation depth in MD simulation (1.7 Å, extracted from force−distance curve) to that of the experimental indentation values (1.3−2.4 Å, estimated using DMT contact model).

Figure 8a shows the deformation field during contact at the maximum force. A smaller tip and substrate is then generated by cutting the original models along a deformation field contour (approximated by fitting an ellipse) that is equivalent to 15% of the maximum tip and sample deformation which happens at the center of contact (Figure 8b). A similar contact simulation is carried out on the modified geometry. The newly cut boundary of the substrate is fixed, and a vertical displacement of 0.18 nm (less than the original displacement to generate the same contact force of 70 nN) is applied vertically. The maximum von Mises stresses and normal compressive stresses of the modified FE model and the original one are listed in Table 4. There is about 1% difference between the maximum contact stresses of the two models with the same contact force. The differences in the stress fields are negligible considering the significant reduction in size of the model.

Molecular Dynamics Simulations. The a-C:H system is generated by producing a diamond surface measuring $2.5 \times 2.5 \times 10$ nm^3 and replacing 35% of the carbon atoms randomly with hydrogen atoms. The AIREBO potential is used to melt the carbon/hydrogen mixture by heating to 8000 K using a Langevin thermostat while holding the bottom 0.65 nm rigid to maintain the structure of the system. A rigid diamond slab is also placed 1.5 nm above the surface to keep the heated atoms from floating away into vacuum. Additionally, periodic boundary conditions are applied in x and y directions so that the system retains its shape. After the surface is melted, the system is minimized to 0 K for 10 ps. The system is then replicated in the lateral directions so that the final measurement of the system is $10 \times 10 \times 10$ nm^3, and the system is minimized again to 0 K for 10 ps. The AIREBO potential as implemented in the LAMMPS[24] molecular dynamics simulator (http://lammps.sandia.gov) is used for the larger simulations to use parallel processing, which significantly speeds up simulation time. Once the system is equilibrated, the equation of an ellipse is used to cut the material to generate

TABLE 4. Elastic Indentation Depth and Resulting Contact Force and Stress of the Original and Modified FE Model

	original model	modified model	error (%)
elastic indentation (nm)	0.21	0.18	
contact force (nN)	69	67	2.9
maximum normal stress at the contact (GPa)	10.4	10.3	1.0
maximum von Mises stress in the tip (GPa)	6.3	6.4	1.6

a geometry determined by the modified FE model shown in Figure 8b. The bottom 0.74 nm of the tip is cut according to a power law equation:

$$z = \frac{x^2 + y^2}{2R} \quad (5)$$

where R (=15 nm) is the radius of curvature of the tip; x and y are Cartesian coordinates in the lateral directions; and z represents the height of the tip. The final geometry of the tip is shown in Figure 9a.

Care is taken so that the cut tip does not include atoms that were held rigid in a diamond structure during the equilibration process. After the tip is cut, the system is minimized to 0 K and then heated in 50 K increments for 10 ps each until the final temperature reaches 300 K. The system expands slightly during this process, so the final measurements of the tip are about 10 nm wide and 8.5 nm tall. The tip model contains 46 947 atoms (67% carbon, 33% hydrogen) which are mostly sp^2-hybridized (77.3%). The rest of the atoms are 7.1% sp- and 15.3% sp^3-hybridized, and 0.3% are overcoordinated.

The 3D UNCD surface structure was generated using the method described in an earlier work.[49] The structure was generated using a Voronoi construction, as outlined by Schiotz *et al.*,[50] wherein a set of grain centers are chosen at random. Atoms are then placed around the nearest center to construct a grain with a face-centered cubic lattice with a randomly selected crystallographic orientation. A lattice parameter equal to 0.35625 nm is used for diamond unit cell. Diamond grains and grain boundaries are chosen to be approximately 2 and 0.5 nm, respectively. The system has dimensions of $10 \times 10 \times 10$ nm^3. Periodic boundary conditions are also applied to mimic the sample as a part of the bulk material. To determine which atoms are in the grain boundary *versus* the grains, the atoms were tagged with their coordination number. Carbon atoms in

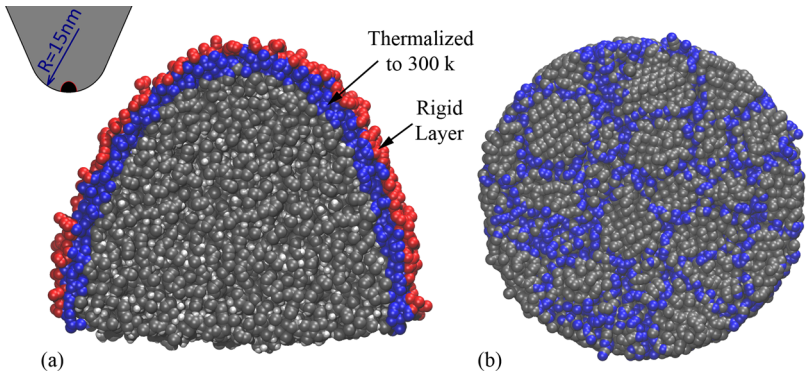

Figure 9. (a) Cross section of the MD simulated a-C:H tip (the black region of the inset refers to the part of the tip that is simulated in MD) and (b) top view of the MD simulated UNCD sample.

diamond have a coordination number of four; therefore, atoms in the UNCD system with a coordination number of four are determined to be part of the grain. Carbon atoms with a coordination number less than four are selected as grain boundaries. To make the grain boundaries amorphous, the atoms tagged as boundaries are relaxed by heating to 8000 K for 10 ps using the AIREBO potential in LAMMPS and a Langevin thermostat while the atoms in the grains are held rigid. After the atoms become amorphous, the energy of the entire system is minimized for 10 ps until the temperature is 0 K. The surface is generated by cutting the bulk model according to the geometry of the UNCD sample shown in Figure 8b. Figure 9b shows the top view of the MD simulated UNCD sample.

After the system is cut, the structure is minimized at 0 K for 10 ps. The system is then incrementally heated to 300 K in steps of 50 K for 10 ps each. During this equilibration process, the dimensions of the system relax from the original values. The final UNCD surface model contains 41 197 carbon atoms and is about 9.2 nm wide and 6.9 nm tall. Finally, the atoms in the outer 0.2−0.3 nm of the surface boundaries are held rigid. The atoms neighboring the rigid layer in 0.7 nm are continually thermalized to 300 K, while the atoms in the center of the ellipsoid are held free.

Contact cycles were run by applying a constant velocity of 50 m/s to the rigid atoms in the a-C:H tip. Two separate pull-back simulations are performed at repulsive contact forces of 20 and 55 nN. Subsequently, two sets of MD simulations with different contact forces of 20 and 55 nN are run as consecutive contact cycles of the 3D UNCD sample with the large a-C:H tip (15 nm radius) comparable to the initial size of the tips used for the experiments (17.8−29.0 nm radius). As shown in Figure 3b, the number of taps required to remove one atom from the tip in AM-AFM experiments is between 100 and 8000 taps, which cannot be realistically simulated by molecular dynamics simulations. Therefore, the UNCD surface here is intentionally left unterminated to promote bond formation and thus tip/sample wear.[51]

Conflict of Interest: The authors declare no competing financial interest.

Acknowledgment. This work was supported by NSF under awards CMMI-0826076, CMMI-0825000, and CMMI-1200019 and STTR grants IIP-0638030 and IIP-0823002 and was partially supported by the Nano/Bio Interface Center through the National Science Foundation (NSF) NSEC DMR08-32802. K.E.R. and P.L.K. acknowledge partial support the Naval Academy Research Office. K.E.R. and J.A.H. acknowledge partial support from the NSF under contracts IAA 1129630, CMMI 0825981, and 1200011. Use of University of Pennsylvania Nano/Bio Interface Center instrumentation is acknowledged. We thank T.D.B. Jacobs for useful and stimulating discussions. We thank K. Sridharan for providing the a-C:H-coated probes.

REFERENCES AND NOTES

1. Young, T. J.; Monclus, M. A.; Burnett, T. L.; Broughton, W. R.; Ogin, S. L.; Smith, P. A. The Use of the PeakForce TM Quantitative Nanomechanical Mapping AFM-Based Method for High-Resolution Young's Modulus Measurement of Polymers. *Meas. Sci. Technol.* **2011**, *22*, 125703.
2. Vasić, B.; Kratzer, M.; Matković, A.; Nevosad, A.; Ralević, U.; Jovanović, D.; Ganser, C.; Teichert, C.; Gajić, R. Atomic Force Microscopy Based Manipulation of Graphene Using Dynamic Plowing Lithography. *Nanotechnology* **2013**, *24*, 015303.
3. Heyde, M.; Rademann, K.; Cappella, B.; Geuss, M.; Sturm, H.; Spangenberg, T.; Niehus, H. Dynamic Plowing Nanolithography on Polymethylmethacrylate Using an Atomic Force Microscope. *Rev. Sci. Instrum.* **2001**, *72*, 136.
4. Bhaskaran, H.; Gotsmann, B.; Sebastian, A.; Drechsler, U.; Lantz, M. A.; Despont, M.; Jaroenapibal, P.; Carpick, R. W.; Chen, Y.; Sridharan, K. Ultra-low Nanoscale Wear through Atom-by-Atom Attrition in Silicon-Containing Diamond-like Carbon. *Nat. Nanotechnol.* **2010**, *5*, 181–185.
5. Gou, L. Q.; Shi, X. L.; Zhao, X. M.; Bai, Y.; Qiao, L. J. Composite Diamond-DLC Coated Nanoprobe Tips for Wear Resistance and Adhesion Reduction. *Surf. Coat. Technol.* **2012**, *206*, 4099–4105.
6. Robertson, J. Diamond-like Amorphous Carbon. *Mater. Sci. Eng., R* **2002**, *37*, 129–281.
7. Loh, O.; Wei, X.; Sullivan, J.; Ocola, L. E.; Divan, R.; Espinosa, H. D. Carbon-Carbon Contacts for Robust Nanoelectromechanical Switches. *Adv. Mater.* **2012**, *24*, 2463–2468.
8. Liu, J.; Notbohm, J. K.; Carpick, R. W.; Turner, K. T. Method for Characterizing Nanoscale Wear of Atomic Force Microscope Tips. *ACS Nano* **2010**, *4*, 3763–3772.
9. Fletcher, P. C.; Felts, J. R.; Dai, Z.; Jacobs, T. D.; Zeng, H.; Lee, W.; Sheehan, P. E.; Carlisle, Ḱ. J. A.; Carpick, R. W.; King, W. P. Wear-Resistant Diamond Nanoprobe Tips with Integrated Silicon Heater for Tip-Based Nanomanufacturing. *ACS Nano* **2010**, *4*, 3338–3344.
10. Gotsmann, B.; Lantz, M. Atomistic Wear in a Single Asperity Sliding Contact. *Phys. Rev. Lett.* **2008**, *101*, 125501.
11. Ronkainen, H.; Koskinen, J.; Likonen, J.; Varjus, S.; Vihersalo, J. Characterization of Wear Surfaces in Dry Sliding of Steel and Alumina on Hydrogenated and Hydrogen-Free Carbon Films. *Diamond Relat. Mater.* **1994**, *3*, 1329–1336.
12. Donnet, C.; Belin, M.; Auge, J. C.; Martin, J. M.; Grill, A.; Patel, V. Tribochemistry of Diamond-like Carbon Coatings in Various Environments. *Surf. Coat. Technol.* **1994**, *68/69*, 626–631.
13. Liu, Y.; Erdemir, A.; Meletis, E. I. A Study of the Wear Mechanism of Diamond-like Carbon Films. *Surf. Coat. Technol.* **1996**, *82*, 48–56.
14. Jiang, J.; Arnell, R. The Effect of Sliding Speed on Wear of Diamond-like Carbon Coatings. *Wear* **1998**, *218*, 223–231.
15. Sha, Z.-D.; Sorkin, V.; Branicio, P. S.; Pei, Q.-X.; Zhang, Y.-W.; Srolovitz, D. J. Large-Scale Molecular Dynamics Simulations of Wear in Diamond-like Carbon at the Nanoscale. *Appl. Phys. Lett.* **2013**, *103*, 073118.
16. Archard, J. F. Contact and Rubbing of Flat Surfaces. *J. Appl. Phys.* **1953**, *24*, 981.
17. Vahdat, V.; Grierson, D. S.; Turner, K. T.; Carpick, R. W. Mechanics of Interaction and Atomic-Scale Wear of

Amplitude Modulation Atomic Force Microscopy Probes. *ACS Nano* **2013**, *7*, 3221–3235.
18. Villarrubia, J. S. Algorithms for Scanned Probe Microscope Image Simulation, Surface Reconstruction, and Tip Estimation. *J. Res. Natl. Inst. Stand. Technol.* **1997**, *102*, 425.
19. Kim, H.; Venturini, G.; Strachan, A. Molecular Dynamics Study of Dynamical Contact between a Nanoscale Tip and Substrate for Atomic Force Microscopy Experiments. *J. Appl. Phys.* **2012**, *112*, 094325.
20. Martínez, N. F.; Kamiński, W.; Gómez, C. J.; Albonetti, C.; Biscarini, F.; Pérez, R.; García, R. Molecular Scale Energy Dissipation in Oligothiophene Monolayers Measured by Dynamic Force Microscopy. *Nanotechnology* **2009**, *20*, 434021.
21. Nejat Pishkenari, H.; Meghdari, A. Influence of the Tip Mass on the Tip−Sample Interactions in TM-AFM. *Ultramicroscopy* **2011**, *111*, 1423–1436.
22. Solares, S. D. Characterization of Deep Nanoscale Surface Trenches with AFM Using Thin Carbon Nanotube Probes in Amplitude-Modulation and Frequency-Force-Modulation Modes. *Meas. Sci. Technol.* **2008**, *19*, 015503.
23. Stuart, S. J.; Tutein, A. B.; Harrison, J. A. A Reactive Potential for Hydrocarbons with Intermolecular Interactions. *J. Chem. Phys.* **2000**, *112*, 6472.
24. Plimpton, S. Fast Parallel Algorithms for Short-Range Molecular Dynamics. *J. Comput. Phys.* **1995**, *117*, 1–19.
25. Melcher, J.; Kiracofe, D.; Hu, S.; Raman, A. *VEDA 2.0 (Virtual Environment for Dynamic AFM)*, 2012.
26. Derjaguin, B.; Muller, V.; Toporov, Y. Effect of Contact Deformations on the Adhesion of Particles. *J. Colloid Interface Sci.* **1975**, *53*, 314–326.
27. Vahdat, V.; Carpick, R. W. Practical Method to Limit Tip−Sample Contact Stress and Prevent Wear in Amplitude Modulation Atomic Force Microscopy. *ACS Nano* **2013**, *7*, 9836–9850.
28. Donnet, C.; Mogne, T. Le; Ponsonnet, L.; Belin, M.; Grill, A.; Patel, V.; Jahnes, C. Respective Role of Oxygen and Water Vapor on the Tribology of Hydrogenated Diamond-like Carbon Coatings. *Tribol. Lett.* **1998**, *4*, 259–265.
29. Erdemir, A. The Role of Hydrogen in Tribological Properties of Diamond-like Carbon Films. *Surf. Coat. Technol.* **2001**, *146−147*, 292–297.
30. Tsuchitani, S.; Sogawa, Y.; Kaneko, R.; Hirono, S.; Umemura, S. Humidity Dependence of Microwear Characteristics of Amorphous Carbon Films on Silicon Substrates. *Wear* **2003**, *254*, 1042–1049.
31. Li, H.; Xu, T.; Wang, C.; Chen, J.; Zhou, H.; Liu, H. Humidity Dependence on the Friction and Wear Behavior of Diamond-like Carbon Film in Air and Nitrogen Environments. *Diamond Relat. Mater.* **2006**, *15*, 1585–1592.
32. Sobota, J.; Grossman, J.; Bursikova, V.; Dupak, L.; Vyskocil, J. Evaluation of Hardness, Tribological Behaviour and Impact Load of Carbon-Based Hard Composite Coatings Exposed to the Influence of Humidity. *Diamond Relat. Mater.* **2011**, *20*, 596–599.
33. Ronkainen, H.; Holmberg, K. In *Environmental and Thermal Effects on the Tribological Performance of DLC Coatings*; Donnet, C., Erdemir, A., Eds.; Springer Science: New York, 2008; pp 172−177.
34. Konicek, A.; Grierson, D.; Gilbert, P.; Sawyer, W.; Sumant, A.; Carpick, R. Origin of Ultralow Friction and Wear in Ultrananocrystalline Diamond. *Phys. Rev. Lett.* **2008**, *100*, 235502.
35. Konicek, A. R.; Grierson, D. S.; Sumant, A. V.; Friedmann, T. A.; Sullivan, J. P.; Gilbert, P.; Sawyer, W. G.; Carpick, R. W. Influence of Surface Passivation on the Friction and Wear Behavior of Ultrananocrystalline Diamond and Tetrahedral Amorphous Carbon Thin Films. *Phys. Rev. B* **2012**, *85*, 155448.
36. Pastewka, L.; Pou, P.; Pérez, R.; Gumbsch, P.; Moseler, M. Describing Bond-Breaking Processes by Reactive Potentials: Importance of an Environment-Dependent Interaction Range. *Phys. Rev. B* **2008**, *78*, 161402.
37. Jacobs, T. D. B.; Gotsmann, B.; Lantz, M. A.; Carpick, R. W. On the Application of Transition State Theory to Atomic-Scale Wear. *Tribol. Lett.* **2010**, *39*, 257–271.
38. Jacobs, T. D. B.; Carpick, R. W. Nanoscale Wear as a Stress-Assisted Chemical Reaction. *Nat. Nanotechnol.* **2013**, *8*, 108–112.
39. D'Acunto, M. Theoretical Approach for the Quantification of Wear Mechanisms on the Nanoscale. *Nanotechnology* **2004**, *15*, 795–801.
40. Johnson, K. L. *Contact Mechanics*; Cambridge University Press: Cambridge, UK, 1985.
41. Luan, B.; Robbins, M. O. The Breakdown of Continuum Models for Mechanical Contacts. *Nature* **2005**, *435*, 929–932.
42. García, R.; Paulo, A. S. Attractive and Repulsive Tip−Sample Interaction Regimes in Tapping-Mode Atomic Force Microscopy. *Phys. Rev. B* **1999**, *60*, 4961–4967.
43. Bares, J. A.; Sumant, A. V.; Grierson, D. S.; Carpick, R. W.; Sridharan, K. Small Amplitude Reciprocating Wear Performance of Diamond-like Carbon Films: Dependence of Film Composition and Counterface Material. *Tribol. Lett.* **2007**, *27*, 79–88.
44. Marques, F. C.; Lacerda, R. G.; Champi, A.; Stolojan, V.; Cox, D. C.; Silva, S. R. P. Thermal Expansion Coefficient of Hydrogenated Amorphous Carbon. *Appl. Phys. Lett.* **2003**, *83*, 3099–3101.
45. Liu, J.; Grierson, D. S.; Moldovan, N.; Notbohm, J.; Li, S.; Jaroenapibal, P.; O'Connor, S. D.; Sumant, A. V.; Neelakantan, N.; Carlisle, J. A.; *et al.* Preventing Nanoscale Wear of Atomic Force Microscopy Tips through the Use of Monolithic Ultrananocrystalline Diamond Probes. *Small* **2010**, *6*, 1140–1149.
46. Sader, J. E.; Chon, J. W. M.; Mulvaney, P. Calibration of Rectangular Atomic Force Microscope Cantilevers. *Rev. Sci. Instrum.* **1999**, *70*, 3967–3969.
47. Hu, S. Nonlinear Dynamics and Force Spectroscopy in Dynamic Atomic Force Microscopy, Ph.D. Thesis, Purdue University, West Lafayette, IN, 2007; pp 74−101.
48. Adiga, V.; Sumant, A.; Suresh, S.; Gudeman, C.; Auciello, O.; Carlisle, J.; Carpick, R. Mechanical Stiffness and Dissipation in Ultrananocrystalline Diamond Microresonators. *Phys. Rev. B* **2009**, *79*, 245403.
49. Adiga, S. P.; Adiga, V. P.; Carpick, R. W.; Brenner, D. W. Vibrational Properties and Specific Heat of Ultrananocrystalline Diamond: Molecular Dynamics Simulations. *J. Phys. Chem. C* **2011**, *115*, 21691–21699.
50. Schiotz, J.; Di Tolla, F. D.; Jacobsen, K. W. Softening of Nanocrystalline Metals at Very Small Grain Sizes. *Nature* **1998**, *391*, 561–563.
51. Ryan, K. E.; Keating, P. L.; Jacobs, T. D. B.; Grierson, D. S.; Turner, K. T.; Carpick, R. W.; Harrison, J. A. Simulated Adhesion between Realistic Hydrocarbon Materials: Effects of Composition, Roughness, and Contact Point. *Langmuir* **2014**, *30*, 2028–2037.